JOURNAL OF PROPULSION AND POWER
Vol. 21, No. 5, September–October 2005

Characterization of 40-Centimeter Microwave Electron Cyclotron Resonance Ion Source and Neutralizer

John E. Foster* and Michael J. Patterson*
NASA John H. Glenn Research Center at Lewis Field, Cleveland, Ohio 44135

Discharge characteristics of a 40-cm, 2.45-GHz electron cyclotron resonance ion thruster discharge chamber and neutralizer were acquired. Thruster bulk discharge plasma characteristics were assessed using a single Langmuir probe. An estimate of the total extractable ion current was measured as a function of input microwave power and flow rate. Additionally, radial ion current density profiles at the thruster's exit plane were characterized using five equally spaced Faraday probes. Distinct low- and high-density operating modes were observed as discharge input power was varied from 0 to 200 W. In the high mode, extractable ion currents as high as 0.82 A were measured. Neutralizer emission current was characterized as a function of flow rate and microwave power. Neutralizer extraction currents as high as 0.6 A were measured.

Nomenclature

A_g = ion grid collection area, m^2
e = 1.6×10^{-19}, C
k = 1.38×10^{-23} J/K
M_i = ion mass, kg
m_e = 9.11×10^{-31} kg
n = plasma density, number/m^3
T_e = electron temperature, eV
Γ = ion current density, A/m^2
ω_c = plasma cutoff frequency, rad/s
ω_{ce} = electron cyclotron frequency, rad/s
ω_p = plasma frequency, rad/s
ω_μ = microwave excitation frequency, rad/s

Introduction

PROPULSION systems capable of providing very high specific impulse (6000–9000 s) are desirable as primary propulsion options for long-term missions to the outer planets and beyond. Gridded ion thrusters systems are capable of satisfying such mission requirements. Ion thruster systems used for such an application will be required to operate continuously for perhaps as long as 5–10 years (Refs. 1 and 2). Such long continuous operation times place stringent lifetime requirements on thruster components and subsystems.

In general, thruster lifetime is limited by essentially four potential failure modes: 1) discharge cathode failure, 2) neutralizer failure, 3) ion optics failure, and 4) electron backstreaming. Failure modes 1 and 2 are related primarily to hollow cathode failure. Failure mode 3 is related to screen and accelerator grid structural degradation via erosion, as well as grid-to-grid shorts arising from such erosion phenomena. Electron backstreaming becomes more and more of a problem as accelerator grid apertures widen due to erosion. High levels of backstreaming electrons can destroy the discharge cathode. One potential solution to this problem is the use of a magnetic grid.[3] Potential design solutions also exist for increasing the lifetime of the ion optics, such as the use of low sputter yield electrode materials such as titanium[4] or carbon[5] or by simply increasing the electrode thickness.[6] Hollow cathode failure can occur after prolonged operation due physical erosion or the depletion of barium in the insert brought on by barium diffusion and subsequent evaporation or the formation tungstates that tie up the barium. Because of such phenomena, ion thruster hollow cathodes have a life of order 28,000 h (Ref. 7), which is not sufficient for those missions requiring more than 3 years of continuous thruster operation. Reservoir cathode approaches have recently been proposed as a means of addressing barium depletion issues associated with conventional hollow cathodes.[8] In a typical reservoir cathode, the barium source is separate from the actual emitter. Although this approach has demonstrated considerable life in vacuum tube applications, it is not yet clear how extended operation in the plasma environment of an ion thruster discharge will affect the device.[9] In addition to ion bombardment of the emitter, physical sputtering of the cathode assembly would still be present.

In an effort to eliminate the lifetime issues associated with conventional hollow cathodes, electrodeless plasma production approaches were investigated.[10,11] Of the electrodeless approaches investigated, microwave electron cyclotron resonance (ECR) discharge was selected as the plasma-generation method based on a parametric comparison with other electrodeless plasma production approaches.[10] In the ECR process, electrons resonantly absorb energy from an imposed electromagnetic field at the electron cyclotron frequency. At resonance, the electrons can gain energy continuously

$$\omega_\mu = \omega_{ce} \tag{1}$$

This resonant process takes place on surfaces of constant $\boldsymbol{B}$ (where $B = 875$ G in the case of 2.45 GHz) that are established by the magnetic circuit. The hot electrons produced during this process ionize neutral gas, thereby generating the discharge plasma completely electrodelessly. This approach has been successfully implemented on the Institute for Space and Astronautical Sciences MUSES-C asteroid rendezvous spacecraft in which microwave ion thrusters (400 W) were used for primary propulsion.[12]

The application of ECR to generate the ion thruster discharge plasma has also been investigated by NASA in the past. A 30-cm ECR ion engine was studied by a NASA-contracted activity in the 1980s. During this effort, ECR plasma sources with discharge losses <150 W/A (5 GHz) were tested.[11] The primary focus of this past effort was to determine the feasibility and technical challenges associated with the development an ECR ion thruster. This work focused on discharge-only operation (0–500 W discharge power) as a means to understand and optimize discharge performance. The present microwave ion thruster development activity focuses on the development of an intermediate-power ion thruster system (40 cm, 1–5 kW). In this regard the goal of this activity is to develop an extremely long-life version of the NASA Evolutionary Xenon Ion

Presented as Paper 2003-5012 at the AIAA/ASME/SAE/ASEE 39th Joint Propulsion Conference and Exhibit, Huntsville, AL, 20 July 2003; received 2 September 2003; accepted for publication 10 May 2004.

*Research Engineer, On Board Propulsion and Power Branch. Member AIAA.

Thruster.[13] The primary application of such a system would be solar electric propulsion missions requiring extremely long thrusting times.

The microwave thruster described in this work uses 2.45 GHz as the plasma excitation frequency. Because 2.45-GHz microwave generators are readily available, this operating frequency affords one a cost effective means of mapping out general operation characteristics of a large, multipole ECR plasma source. Issues such as magnetic circuit optimization, dc isolation, impedance matching, and power injection issues can all be studied using this test-bed plasma source.

The beam current design goal for this 2.45-GHz ECR test-bed ion thruster is 1.1 A at a microwave input power of 300 W or less. The 1.1-A beam current goal corresponds to the maximum ion current density for this thruster diameter at this particular microwave frequency. In general, the maximum extractable current is a function of the plasma density and the electron temperature:

$$\Gamma = 0.61 \cdot e \cdot n \cdot \sqrt{k \cdot T_e / M_i} \tag{2}$$

Thermal, background electron temperatures are expected to range between 2 and 5 eV. To first order, the maximum plasma density obtainable depends primarily on microwave excitation frequency. The plasma in the ECR zones can reach a maximum density determined by the condition where the microwave frequency equals the local plasma frequency: $\omega_\mu = \omega_p$. Normally, at plasma frequencies higher than the microwave frequency, the microwaves are no longer absorbed, but reflected instead. Under normal conditions, bulk plasma density does not appreciably exceed this cutoff plasma density value.

Future work will require a microwave frequency of 5 GHz or greater to achieve the required beam currents for the 5-kW operating condition.[13] The higher frequency will also significantly reduce the discharge losses.[9] Lessons learned from the 2.45-GHz source such as method of power injection and ring cusp magnetic circuit design will be implemented in the 5-GHz design. With the exception of the reduced waveguide dimensions, implementation of microwave injection approach should be identical at both frequencies. The magnetic circuit associated with containment of the discharge plasma should also be identical because the primary role of the circuit is to establish ECR heating zones and contain the plasma and circulate ECR heated electrons between magnet rings to generate plasma at the periphery. The magnets used at the microwave injection port and the magnetic circuit in general are expected to use the same type of rare earth permanent magnets. These magnets have surface field strengths well in excess of that required to generate ECR at both 2.45 and 5 GHz (875 G and 1.785 kG, respectively).

In parallel with this development activity is an effort to develop a microwave neutralizer. The microwave ECR plasma cathode would be developed as a replacement for the conventional hollow cathode neutralizer, thereby eliminating the barium depletion failure mode associated with hollow cathodes. Flight-qualified microwave neutralizers have been demonstrated at electron emission currents up to 150 mA (MUSES-C).[12,14] Considerably higher electron emission currents will be required for the 5–10 kW engine (1–3 A) (Ref. 13). Such high emission currents have been demonstrated by ECR plasma cathodes used for ground-based plasma processing applications.[15] These sources, however, demonstrated such high electron currents only when operated inside a discharge chamber. These electron sources also operate at 2.45 GHz.

The discharge plasma of the 40-cm ECR source studied in this work was characterized in preparation for operation with beam extraction. This characterization study was conducted over an input microwave power range of 0–200 W. Input microwave discharge power levels were limited by the heat rejection capacity of the microwave transmission lines. The findings of this investigation are reported here. Additionally, microwave neutralizer operation was characterized. The neutralizer's emission current as a function of discharge power and flow rate was assessed in a series of independent experiments. Findings from these tests are also reported.

Experimental Setup

The 40-cm microwave ECR discharge testing took place in an aluminum vacuum facility approximately 2.2 m in diameter and 7.9 m in length. The pumping train includes a two-stage blower system backed by a roughing pump, a turbomolecular pump, and seven helium cryopumps. The approximate pumping speed was 110,000 l/s on xenon at 1×10^{-6} torr. The nominal base pressure was 1.3×10^{-5} Pa (1×10^{-7} torr), whereas background pressure at the highest flow rate condition investigated was 6.6×10^{-4} Pa (3×10^{-6} torr).

The ring cusp magnetic circuit consisted of samarium cobalt magnet rings of alternating polarity. Primary ECR heating occurs in regions just above the magnetic cusps.[8,11] Here the magnetic field is of sufficient value that intense electron heating can occur. Xenon gas was injected into the discharge chamber using a reverse feed plenum located roughly midway in the cylindrical section of the partial conic discharge chamber. Additional detail regarding the ring cusp discharge chamber configuration may be found in Ref. 8.

The exit plane of the discharge chamber was terminated using a stainless steel perforated electrode with physical open area fraction similar to that of two-grid ion optics (20%) (Ref. 16). This electrode was biased to ion saturation to determine an estimate of the extractable ion current. The ion grid was also fitted with a series of five equally spaced, radial Faraday probes, measuring 6.35 mm in diameter. The probes were spaced approximately 4.5 cm apart. These probes were biased to ion saturation to assess ion current density uniformity in the plane of the optics. The probe current was measured using an in-line current meter that was accurate to within 0.5 μA. Additionally, a tungsten wire Langmuir probe was mounted inside the discharge chamber. The probe whose tip was approximately 5 mm long and 0.38 mm in diameter was used to assess bulk discharge properties as a function of operating condition. Axially, the probe was located approximately at the midpoint of the cylindrical section, extending radially approximately 11 cm. The probe was driven using a commercially available Langmuir probe power supply. Approximately 10 readings were made at each voltage point during a given sweep. Additionally, the reduced data was the average 10 total sweeps for a given operating point. As acquired using the probe driver, the uncertainty in the plasma density was less than 33%. The magnetic field at the probe tip was approximately 15 G. In this regard, probe analysis corrections to account for strong magnetic effects were not necessary.[17] Because the Langmuir probe was located between two magnet rings, no portion of the tip or body intersected a resonant ECR zone. This also reduced probe perturbations to the discharge plasma. Additionally, because of the high microwave excitation frequency, corrections to the probe current–voltage characteristic is not necessary. Plasma particles in the bulk discharge cannot respond to the high-frequency field. The potential difference between the plasma and the probe potential reduces to the dc plasma case. The uncertainty in the plasma potential was approximately 0.5 V.

Microwave power at 2.45 GHz was introduced on axis into the discharge chamber using a cylindrical waveguide. The cylindrical waveguide attachment contained a sliding short, which was used for impedance matching.[18] The cylindrical waveguide section was excited using a coax to waveguide adapter. The adapter's dominant excitation mode is the rectangular TE_{10}. This mode is converted to the cylindrical TE_{11} mode in the cylindrical microwave launcher section (Fig. 1).[18] Coaxial lines were used to feed power from the microwave magnetron, which was located on the atmosphere side of the tank, to the thruster's coax to waveguide adapter. Also located on the atmosphere side was a circulator to handle reflected power, a directional coupler to sample signals proportional to the forward and reflected power, and a three stub tuner, which was also used for microwave power impedance matching. Forward and reflected power signals were converted to actual power using two microwave power meters. In all cases, the reflected microwave power was less than 20%. The uncertainly in the forward power that actually enters the thruster was estimated at approximately 25%.

Though the microwave magnetron was capable of outputting over 1 kW of continuous wave (cw) microwave power, experiments were

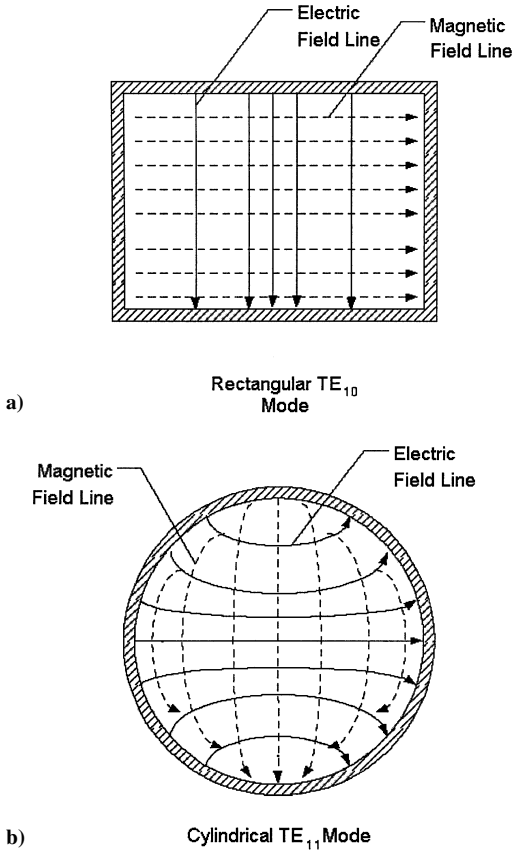

Fig. 1 Cross-sectional view of electromagnetic field patterns inside waveguide for the dominant mode TE_{10} (rectangular) and the dominant mode TE_{11} (cylindrical).

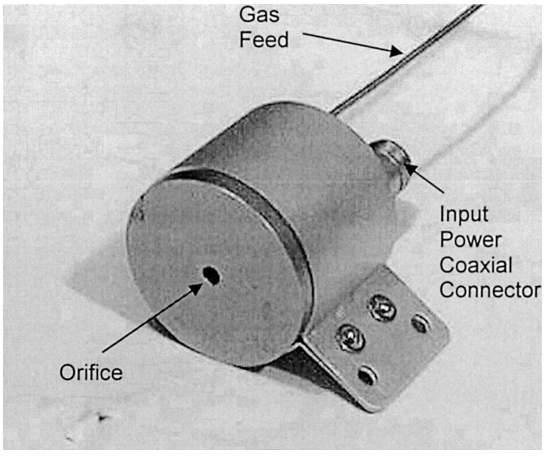

Fig. 2 Microwave neutralizer.

typically limited to less than 250 W due to the limited power handling capability of the microwave cable. To investigate discharge operation at higher discharge powers, a waveguide must be used. Such a system is presently being installed at the VF11vacuum facility in preparation for high-power operation with beam extraction.

Neutralizer testing was performed in a 0.61 m diameter by 0.91 m long stainless steel bell jar with a 0.25-m cryopump. The cryopumped facility had a pumping speed of 1300 l/s (xenon). The facility contained an automated data acquisition and control system, power console, and an integrated high-purity propellant feed system. Base pressure was approximately 10^{-7} torr. During testing, operating pressure ranged between 3×10^{-5} torr at 0.5 standard cm^3 to 1×10^{-4} torr at 3 sccm of xenon. The neutralizer, shown in Fig. 2, consisted of a 3.5-cm-diam mild steel discharge chamber with a 3-mm-diam orifice. A gas plenum ring was used to inject the xenon gas into the device. The neutralizer contained an electrically isolated spiral antenna made of molybdenum. The antenna is immersed in a magnetic field greater than the for ECR resonance value at 2.45 GHz. This configuration assures the ECR heating zone accessibility, thereby eliminating cutoff issues.[19] The desired magnetic field is generated by two samarium cobalt magnet rings. In the neutralizer tests, a molybdenum electrode was placed approximately 7 cm downstream of the neutralizer to collect the electron current. Additional details regarding the microwave neutralizer configuration may be found in Ref. 8. For all discharge tests conducted in this work, both the main discharge and the neutralizer were left at ground potential. In the case of the neutralizer, the anode collection plate was biased positively with respect to ground to extract the electron current.

Experimental Results

40-Centimeter Discharge

Discharge operation of the 40-cm source was characterized as a function of microwave input power. The flow rate was set at approximately 20 standard cm^3, and the net microwave input power was varied between 0 and 200 W.

Discharge Appearance

Because the microwave power was introduced on centerline, the microwave propagation vector $\boldsymbol{k}$ is directed along the discharge axis. In this regard, the vector is parallel to the magnetic field vector at the surface of the most upstream ring, magnet ring 1, 90 deg θ_c deg (where θ_c is the conical section angle) with respect to the magnetic field vector at ring 2, perpendicular to the magnetic field vector at rings 3 and 4, located in the cylindrical section, and parallel to the magnetic field vector at the surface of ring 5. The orientation of the propagation vector with respect to the magnetic field vector as well as the vector's approach direction both determine what type of electron heating if any at all will occur. Figure 3 is the magnetic field strength vs plasma density.[19] Figure 3 shows two relevant modes of wave absorption (resonance) that can take place in this discharge chamber configuration. These modes include the right-hand circularly polarized mode (RHCP) and the upper hybrid frequency mode.

If the propagation vector is parallel to the magnetic field vector with the microwave radiation approaching the ECR zone from the high field side, then absorption will always take place as indicated in Fig. 3. In this case, the absorption occurs at the RHCP resonance where $\omega_\mu = \omega_{ce}$. Under these conditions, reflected microwave power is minimal, and overdense plasma production is possible. Overdense refers to plasma density in which the plasma frequency exceeds the radiation field frequency. Normally under such conditions, the radiation is simply reflected; however, the dispersion relation for

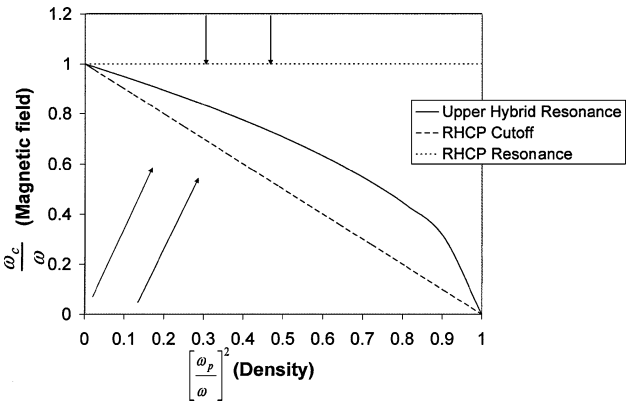

Fig. 3 Clemmow-Mollaly-Allis (CMA) diagram of various resonances and cutoffs for specified plasma density and magnetic field: upward pointing arrows, waves approaching ECR resonance from weak field side, and downward pointing arrows, approach from the high-field side.

RHCP absorption allows for the propagation of the radiation to the heating site.[19] Though this form of heating is most desirable, it is not usually straightforward to design using permanent magnets-only configurations.[20] Conditions for this form of absorption exist at magnet ring 1. The upper hybrid heating resonance (Fig. 3) condition can be satisfied at rings 2, 3, and 4 (Ref. 19). Here, the microwaves approach the resonant zones perpendicular to the magnetic field. Additionally, the $\boldsymbol{k}$ vector approach to the heating zone is from the weak magnetic field side.[21] At plasma densities corresponding to plasma frequencies above the microwave excitation frequency, this absorption process should cease. In reality, microwaves can tunnel through the separation between the cutoff and the resonance, thereby allowing for the formation of densities above the critical plasma density (as defined at the condition where plasma frequency equals microwave frequency). Absorption at ring 5 is likely due to a combination of upper hybrid frequency production and tunneling to the RHCP resonance.

Note that microwave radiation not absorbed can be converted to other modes by scattering (which changes the direction of the propagation vector) and that other microwave radiation modes are more or less absorbable via the processes described earlier.

The mentioned absorption processes are useful in interpreting the discharge appearance. The discharge appearance reflects qualitatively what absorption modes are active in the discharge chamber. The 40-cm discharge appears to have several distinct modes of operation. In general at input discharge powers less than 100 W, the ECR plasma production is localized primarily to the most upstream magnet rings (conical section). In this regard, at low powers, upper hybrid resonance can be expected to dominate. As the power approaches 100 W, an annular region near the pole piece magnet ring (ring 5) becomes luminous as well. This low-power discharge condition is shown in Fig. 4a. In this mode, the discharge overall is fairly dim, but its brightness intensifies with increasing flow rate (internal pressure). This increase is attributed to increased neutral–electron collisions, which tend to generate a secondary discharge plasma in the bulk. In any case, the ECR action locally at the rings is very intense in contrast to the bulk of the discharge. The core plasma of these rings has a white tone, indicating a very intense and localized interaction between very hot electrons and neutral gas. The brightening of the bulk discharge with increasing power in this mode is most likely due to increased production of hot electrons that ionize gas at and between magnetic cusps, ultimately diffusing into the main volume to excite/ionize neutrals there.

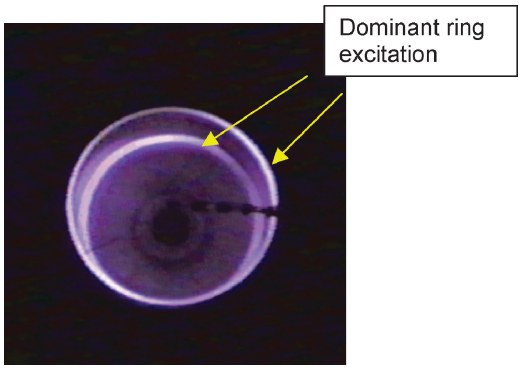

Fig. 4a Low-power discharge operation; discrete ECR ring plasma production visible in the conical section and at the pole piece.

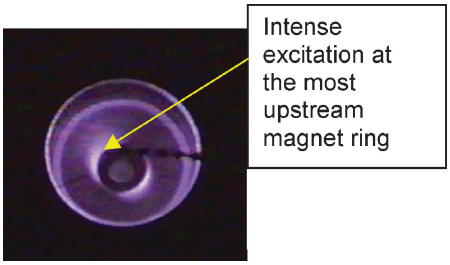

Fig. 4b Intermediate mode just before transition into high mode, most upstream magnet ring discharge ushers in onset of high mode.

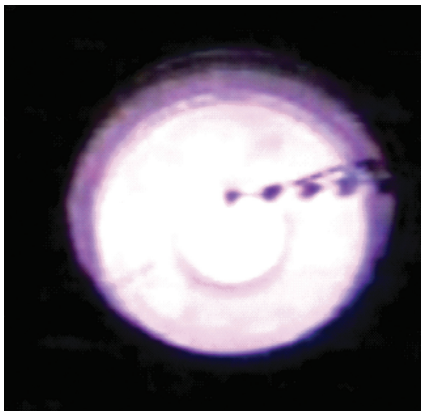

Fig. 4c High mode operation; distinct ECR sites at the magnet rings absent.

As the microwave power is increased between 100 and 150 W, an intense plasma glow is observed at the most upstream ring (ring1, near waveguide opening) as well. This plasma production is shown in Fig. 4b. This plasma production mechanism is likely due to RHCP heating. The bulk discharge brightness also increases with the appearance of this new mode. With increasing microwave power >150 W, the discharge jumps into an operating mode dominated by volume excitation. In this mode (Fig. 4c), the emission intensity at distinct ECR plasma production sites at the magnet rings are washed out by the intense volume glow. It is postulated that the jump into this mode is due to RHCP heating and possibly anomalous heating at the most upstream ring.[19,21] The presence of plasma at this ring in the intermediate microwave power mode (Fig. 4b) provides a medium for the RHCP radiation to couple into. Overdense plasma production can then take place at this ring. Plasma production improves with increasing input microwave power, ultimately culminating in the bright discharge shown in Fig. 4c. As will be shown later, this mode is characterized by high density and high uniformity.

Discharge Plasma Properties

Plasma characteristics such as bulk density, plasma potential, and electron temperature were measured over the power range investigated. Average extractable ion current at the discharge chamber exit plane was measured by biasing the ion optics simulator grid. In addition to these measurements, radial button probes were used to measure the ion current uniformity at the exit plane.

The plasma measurements acquired were consistent with the visual observations made as net input microwave power was increased from 0 to 200 W. Figure 5 shows the variation in the bulk plasma density as measured using a Langmuir probe between 0 and 200 W at a flow rate of approximately 20 sccm. Note that there is a distinct jump in plasma density as microwave power increases appreciably above 140 W. This jump is associated with the visually observed transition to the full volume plasma production mode. In the low mode, plasma density increases very slowly with increasing microwave power with an average increase in density of $1.11 \times 10^7/\text{cm}^3 \cdot \text{W}$. As shown in Fig. 5, the plasma density increases by over a factor of five as the power increases from 140 to 170 W. The rate of growth in density with increasing discharge power in the high mode is considerably higher than low mode growth. Plasma density growth in the high mode is nearly linear, with increasing microwave power at a rate of increasing $8.45 \times 10^7/\text{cm}^3 \cdot \text{W}$ in this regime.

The plasma potential was observed to drop as the plasma jumps from low mode to high mode. Figure 6 shows the drop of a factor

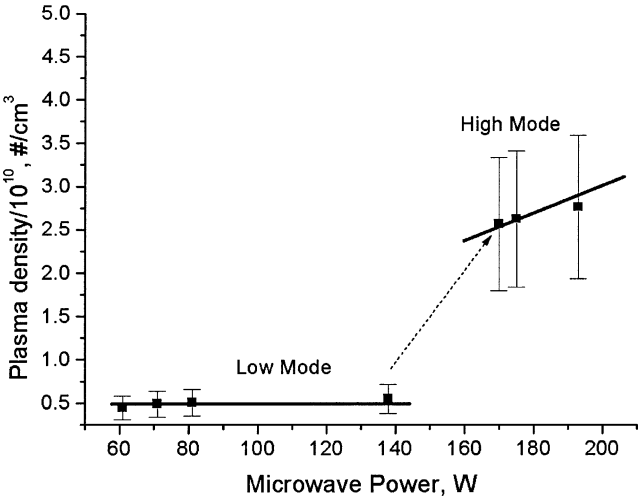

Fig. 5 Bulk plasma density variations showing distinct mode transition.

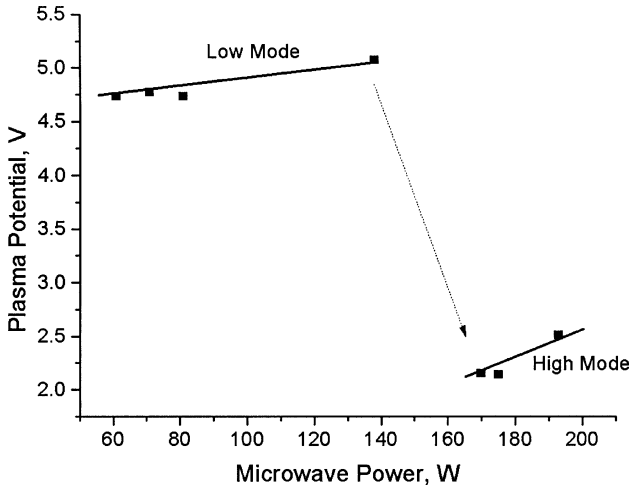

Fig. 6 Plasma potential variations with microwave power.

of two as power is increased from 0 to 200 W. This transition also proceeds in concert with the increases in plasma density. The low measured plasma potential suggests a plasma to screen grid potential difference of order 1/10 that of the NASA Solar Electric Propulsion Technology Application Readiness (NSTAR) thruster. In general, reduced plasma potential is desirable for ion thruster operation in that the energy of ions falling out of the discharge into the screen grid is reduced.

The electron temperature does not vary appreciably as the plasma transitions from high mode to low mode. Its value was approximately 2 eV over the power range investigated here at this flow rate. The relative flatness in the electron temperature with increasing input power suggests that the improved discharge performance in the high mode is not so much a consequence of better heating of the electrons, but of an increase in the number of regions where plasma production is taking place.

It is postulated that RHCP absorption at ring 1 may play a major role in the improved discharge characteristics in the high mode. Because the Langmuir probe point measurements sampled the bulk plasma, these data should be representative of volume plasma processes. In this regard, the gradients measured as power is increased represent improved volume plasma production with the transition into the high mode. The highest plasma density condition observed in the high mode corresponded to a plasma density 50% less than the cutoff frequency 7.45×10^{10}#/sccm, indicating that the plasma density was still below cutoff. Near the rings, the plasma density may be much larger than that measured by the Langmuir probe,

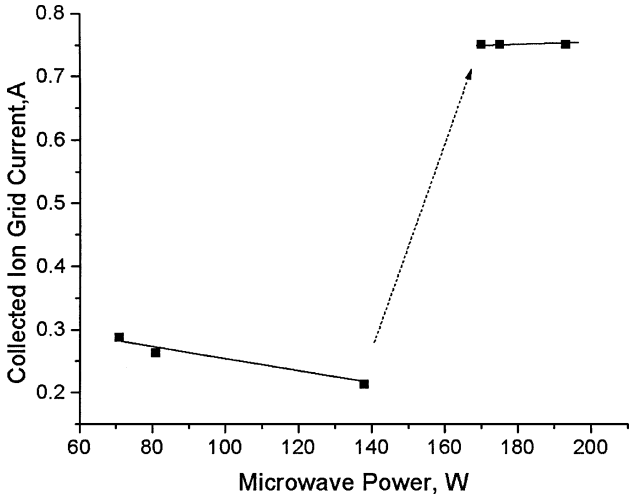

Fig. 7 Variations in the grid ion current as function of microwave power.

which sampled the bulk of the discharge, near the centerline. In this regard because the microwave frequency was greater than the cutoff frequency at these plasma densities in the main volume discharge, microwave power can indeed still propagate through the bulk and be absorbed at the ECR sites. Given the slope of change in plasma density with increasing discharge power, it is expected that the cutoff density would be obtained in the bulk plasma at a microwave input power of 700 W. It follows then that increasing the input microwave power should bring about further increases in the plasma density. This study was limited to operating microwave input powers $<$250 W due to coax cable overheating.

The ion current collected at the biased ion optics simulator grid also increased significantly as the discharge transitioned from low mode to high mode. Figure 7 shows variations in the ion current collected at the grid at roughly 20 sccm. Behavior similar to that observed in the plasma density and plasma potential with increasing microwave power is observed in the grid current, but there are some differences. At this fixed flow rate, the grid current in high mode did not increase appreciably with increasing discharge power. The grid current's average value was approximately 0.75 A. This result suggests that the spatial plasma density distribution might be changing with increasing microwave power. The density may be increasing in the bulk and decreasing in the wings so that the net change in current collected at the grid is nearly zero.

Changes in the current density distribution as measured using radial probes mounted on the ion optics simulation electrode seem to support this notion. Figure 8 illustrates variations in the ion current density profile as the plasma goes from "high mode" to "low mode." Clearly there is a distinct change in the ion current distribution with increasing microwave power. In the "low mode" the ion current density is peaked at the edges, near the discharge chamber walls. The very hollow, "donut-like" distribution associated with the "low mode" is appreciably filled in the "high mode." The progression into the "high mode" with increasing power yields a density profile similar to that observed in DC ion thrusters. The observed absence of a peaked.

The measured current density distribution is consistent with the visual observations. In the low mode, the most prominent plasma excitation occurs at the rings. It is, therefore, to be expected that the current density would be peaked at the wings in the low mode. The observed volume excitation in the high mode is consistent with the improved current density uniformity.

In this investigation, grid currents up to 0.82 A were achieved at 12.5 sccm. This grid current is within 7 percent of the equivalent amperes of input xenon gas. Here equivalent amperes is defined as the product of the ratio of the input xenon mass flow rate to the mass per xenon atom and the elementary charge of an electron. It follows from mass conservation that this parameter represents the

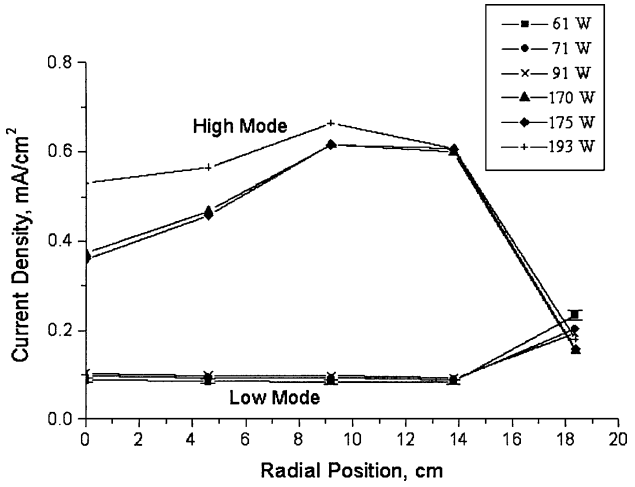

Fig. 8 Radial ion current density variations with changes in microwave power.

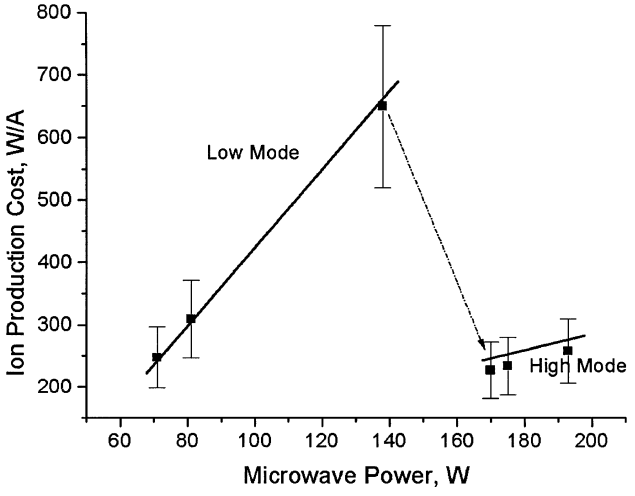

Fig. 9 Variation in the ion production costs with input microwave power; distinct behavior change from high mode to low mode.

maximum beam current that can be extracted. The ratio of the ion beam current to the equivalent ampere flow rate is equal to the discharge propellant utilization. Because this calculation does not take into account ingestion of neutrals formed by ions recombining on the grid and reentering the discharge, in this work this ratio represents an upper limit on the propellant utilization. These data suggest an uncorrected utilization of order 93%. The collected grid current is consistent with an average plasma density that is approximately 75% of the microwave cut-off limit. Because bulk plasma densities were of order a factor of two times lower than the cut-off value, the large current measured at the grids may be due to an increase in the electron temperature near the grid. These data also suggest that large increases in discharge power beyond 200 W may not be necessary to achieve the target of a 1 A ion beam.

The estimated discharge efficiency upper limit as characterized by ion production cost (discharge power/ion current) is plotted in Fig. 9 for the 20 sccm flow condition. As can be seen here, there is also a distinct change in functional behavior as power is increased. The "low mode" is characterized as high ion production costs with a larger slope indicating higher losses with increasing input power. The sudden jump to the "high mode" is characterized by reduced ion production costs (~200 W/A) and a much shallower slope indicating the discharge efficiency degrades with increasing power at a lesser rate than in "low mode." It is expected that the ion production costs can be improved by either increasing the microwave frequency or by increasing the input power to achieve anomalous heating.[22]

Preliminary Neutralizer Characterization

The microwave neutralizer featuring an internal antenna also operating at 2.45 GHz was also characterized. The primary objective of this investigation was to minimize required neutralizer flow rate and electron extraction voltage while at the same time maximize the output electron emission current. Minimizing the gas flow rate improves specific impulse and overall thruster efficiency. Such reductions also decrease the population of those neutrals that travel to the ion optics region and participate in charge exchange collisions. Reducing the extraction or neutralizer coupling voltage minimizes neutralizer erosion rates by reducing energy at which ions created in the neutralizer plasma impact the device.

In these experiments, a planar anode placed downstream of the neutralizer, was used to extract the electron current. Figure 10 shows qualitative features of the neutralizer's operation. In general, as shown in Fig. 10, the neutralizer operates in the so-called plume mode. This mode of operation is similar to that observed with similar devices.[14,22] In general, additional ionization of gas escaping from the neutralizer contributes to the collected electron current. Such ionization generates a plasma bridge, which reduces the impedance between the device and the anode. This plume ionization necessitates some minimum voltage drop between the neutralizer and anode (or ion beam in the case of an actual ion thruster application). In this work, it was found that 50–56 V was the minimum voltage range at which appreciable electron current (>0.3 A) could be extracted.

Figure 11 illustrates variations in electron extraction voltage between the neutralizer and the anode as a function of xenon flow rate. These data were obtained by fixing the net input microwave power to approximately 80 W and setting the electron emission current to 0.3 A. As can be seen in Fig. 11, the lowest impedance occurs at the highest flow rates, which suggests plume ionization as an important contributor of free electrons. Between 1.5 and 2 sccm, the coupling voltage did not vary appreciably. This relatively flat region is likely attributable to competition between electron temperature cooling and electron ion pair formation, both of which are proportional to the neutral density. Further reductions in neutralizer flow rate gave rise to a linear increase in discharge voltage.

Figure 12 illustrates optimized electron extraction currents as a function of input power at slightly different flow rates. In general, for this device, the highest extracted electron current (at extraction voltages below 60 V) occurred for flow rates between 2 and 3 standard cm.[3] As can be seen in Fig. 12, at flow rates near 3 standard cm^3, the collected electron current increased nearly linearly with increasing input microwave power. The maximum current obtained in these preliminary experiments was approximately 0.6 A. For the cases shown in Fig. 12, the discharge voltage could not be reduced below 56 V. These coupling voltages are somewhat lower than that reported for similar devices (100 V in Ref. 14). Attempts to reduce

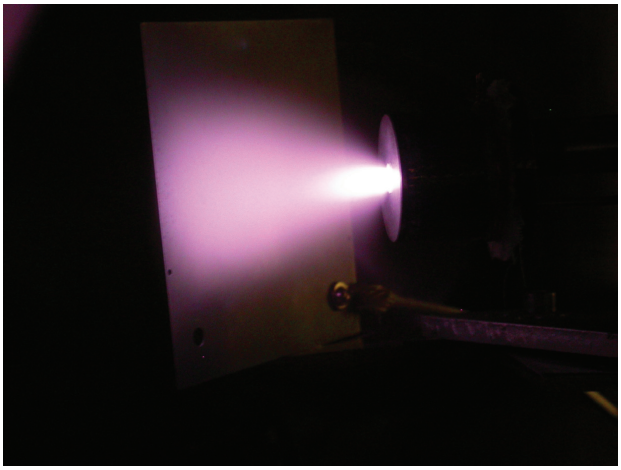

Fig. 10 Microwave neutralizer in operation; plumelike mode discharge.

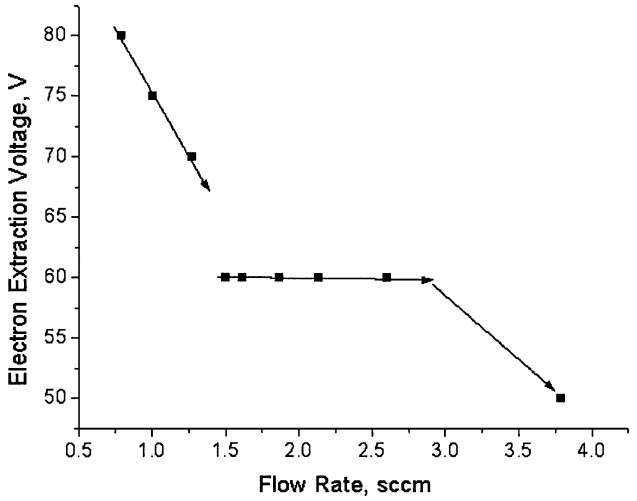

Fig. 11 Variation in extraction voltage with increasing neutralizer flow rate.

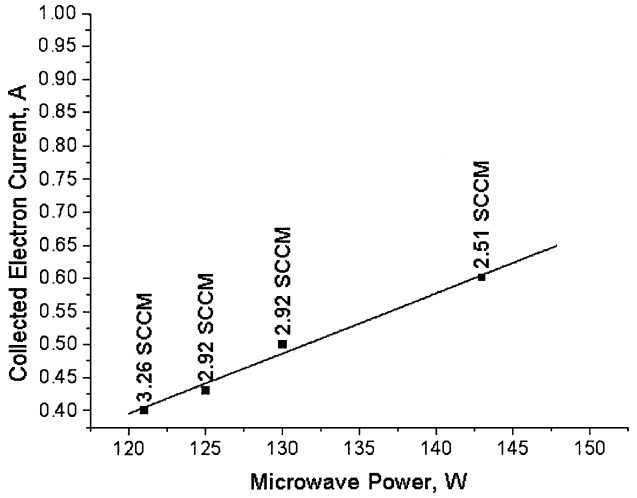

Fig. 12 Collected electron current as function of microwave power and neutralizer flow rate.

the discharge voltage below 56 V resulted in extinguishment of the plasma bridge between the neutralizer and the anode.

The calculated electron–neutral ionization pathlength for 50–56 eV electrons produced in this discharge is well in excess of the discharge interelectrode spacing. In this respect, the minimum discharge voltage is likely due to the role of the local magnetic field produced by the neutralizer. The field in the discharge gap enhances the plume ionization process by reducing the electrons effective collisional mean free path to that of a Larmor radius, which in this case is a length scale less than the interelectrode spacing. This way ionization can take place in the interelectrode gap. This improves the utilization of primary electrons before they are collected at the anode.

Further modifications to the neutralizer's magnetic circuit should allow operation at higher electron currents. These modifications are expected to focus on reducing the transverse component of the magnetic field at the orifice while at the same time leaving the residual field in the gap largely unchanged so that plume ionization is still enhanced. With the resulting increase in the transverse electron diffusion coefficient in the orifice, a modest rise in primary electron current flowing into the interelectrode gap can be expected. Note that the microwave power required to generate a given electron current can be significantly reduced by increasing the excitation frequency above 2.45 GHz. This planned approach should significantly improve performance.

Conclusions

In preparation for testing with beam extraction, discharge characteristics of a 2.45 GHz microwave ECR ion thruster plasma generator and a neutralizer were characterized. The ECR discharge was found to have two distinct operating modes. The "low mode," which is associated with low input microwave power, is characterized as a nonuniform, low plasma density operating mode. The "high mode" is characterized by volume plasma production as evidenced by the visually observed bright, full volume plasma excitation and relatively flat ion current density profiles. Ion currents near the expected maximum (1.1 A) were collected at the grids in the "high mode." Additionally, in the "high mode," the uncorrected propellant utilization was measured to be as high as 93% with associated discharge losses as low as 200 W/A.

The neutralizer, which featured an internal antenna, generated electron currents as high as 0.6 A. The neutralizer was found to require a minimum extraction voltage of 50–56 V for stable plasma bridge formation and electron extraction. Test results indicate that the residual magnetic field in the region between the neutralizer and collection electrode likely enhances plume ionization and thus neutralizer-collection electrode coupling. Higher extracted electron current levels from the neutralizer body should be attainable by straightforward modifications to the orifice magnetic field.

Acknowledgments

The authors would like to thank Bob Roman for the fabrication of the ion source.

References

[1]Shotwell, R., "Carbon–Carbon Grid Development for Ion Propulsion Systems," IEPC Paper 2001-093, Oct. 2001.

[2]Rawlin, V. K., Williams, G. W., and Roman, R. F., "High Specific Impulse, High Power Ion Engine Operation," AIAA Paper 2002-3838, July 2002.

[3]Foster, J. E., Roman, R., Soulas, G. S., and Patterson, M. J., "Magnetic Grid for Electron Backstreaming Mitigation," IEPC Paper 01-221, Oct. 2001.

[4]Soulas, G. C., Foster, J. E., and Patterson, M. J., "Performance of Titanium Optics on a NASA 30 cm Ion Thruster," AIAA Paper 2000-3814, July 2000.

[5]Haag, T., Patterson, M. J., and Soulas, G. C., "Carbon-Based Ion Optics Development at NASA GRC," IEPC Paper 01-094, 27th IEPC, Oct. 2001.

[6]Soulas, G. C., "Improving Total Impulse Capability of the NSTAR Ion Thruster with Thick-Accelerator—Grid Ion Optics," IEPC Paper 01-081, Oct. 2001.

[7]Kovaleski, S. D., Patterson, M. J., Soulas, G. C., and Verhey, T. R., "A Review of Hollow Cathode Testing for the International Space Station Plasma Contactor," IEPC Paper 01-271, 27th IEPC, Oct. 2001.

[8]Polk, J. E., Goebal, D., Brophy, J. R., Beatty, J., Monheiser, J., Giles, D., Hobson, D., Wilson, F., Christensen, J., De Pano, M., Hart, S., Ohlinger, W., Hill, D. N., Williams, J., Wilbur, P., and Farnell, C., "An Overview of the Nuclear Electric Xenon Ion System (NEXIS) Program," AIAA Paper 2003-4713, July 2003.

[9]Dieumegard, D., Tormerre, J. C., Brion, D., and Shroft, A. M., "Life Test Performance of Thermionic Cathodes," *Applied Surface Science*, Vol. 111, Feb. 1997, pp. 84–89.

[10]Foster, J. E., and Patterson, M. J., "Status of Microwave Thruster Development Activity at NASA GRC," AIAA Paper 2002-3837, July 2002.

[11]Goede, H., and Fosnight, V. V., "High Frequency Plasma Generators," NASA-Contract NAS3 22473, Nov. 1981.

[12]Toki, K., Kuninaka, H., Nishiyama, K., Shimizu, Y., and Funaki, I., "Technological Readiness of Microwave Ion Engine System for MUSES-C Mission," International Electric Propulsion Conf., IEPC Paper 01-174, Oct. 2001.

[13]Patterson, M. J., Foster, J. E., Haag, T. W., Pinero, L., Rawlin, V. K., Soulas, G. C., Doehne, M. S., and Roman, R., "Development Status of a 5/10-kW Class Ion Engine," AIAA Paper 2001-3489, July 2001.

[14]Satori, S., Kuniaka, H., Ohtaki, M., and Ishikawa, Y., "Operational Characteristics of Microwave Discharge Neutralizer," International Electric Propulsion Conf., IEPC Paper 97-051, Aug. 1997.

[15]Matsubara, Y., Tahara, S., Janzo, H., and Ishikawa, J., "Development of Microwave Plasma Cathode for Ion Sources," *Review of Scientific Instruments*, Vol. 61, No. 1, 1990, pp. 541–543.

[16]Patterson, M. J., Haag, T. W., Rawlin, V. K., and Kussmaul, M. T., "NASA 30 cm Ion Thruster Development Status," AIAA Paper 94-2849, July 1994.

[17]Sugawara, Minoru, "Electron Probe Current in a Magnetized Plasma," *Physics of Fluids*, Vol. 9, No. 4, 1966, pp. 797–800.

[18]Wheeler, G. J., *Introduction to Microwaves*, Prentice Hall, NJ, 1963, pp. 57–60.

[19]Chen, F. F., *Introduction to Plasma Physics and Controlled Fusion*, Plenum, Press, NY, pp. 126–136.

[20]Toki, H., Fujita, H., Nishiyama, K., Kuninaka, H., Toki, K., and Funaki, I., "Performance Test of Various Discharge Configurations for ECR Discharge Ion Thruster," International Electric Propulsion Conf., IEPC Paper 01-107, Oct. 2001.

[21]Musil, J., "Anomalous Absorption of Intense Electromagnetic Waves in Plasma at High Magnetic Fields," *Plasma Physics*, Vol. 19, 1974, pp. 735–739.

[22]Onodera, N., Takegahara, H., Nishiyama, K., Funaki, I., and Kuninaka, H., "Electron Emission Mechanisms of Microwave Discharge Neutralizer," International Electric Propulsion Conf., IEPC Paper 99-160, Oct. 1999.